Giant Molecular Magnetocapacitance

Yu-Ning Wu, X.-G. Zhang, and Hai-Ping Cheng

Phys. Rev. Lett. **110**, 217205 — Published 22 May 2013

DOI: 10.1103/PhysRevLett.110.217205

Giant Molecular Magnetocapacitance

Yu-Ning Wu[1], X.-G. Zhang[2], and Hai-Ping Cheng[1*]

[1]Department of Physics and the Quantum Theory Project, University of Florida, Gainesville, FL 32611

[2] Center for Nanophase Materials Sciences, Oak Ridge National Laboratory, Oak Ridge, TN 37831-6493

Through investigating the spin-dependent charging energy of nanoscale systems, we introduce a new concept of intrinsic molecular magnetocapacitance (MC). In molecules and nano-size quantum dots that undergo a spin state transition, the MC can be as high as 12%. First-principles calculations demonstrate that in a number of nanoscale systems, the quantum capacitance is highly sensitive to the system spin and charge states. In single molecule junctions, one can exploit molecular MC through the Coulomb blockade effect by modulating the bias voltage and applying an external magnetic field, which turns electron conductance on or off. Detailed analysis on molecular nano-magnet $Mn_3O(sao)_3^-(O_2CMe)(H_2O)(py)_3$ shows a 6% MC with a switching field of ~40 T. Its MC can be further enhanced to 9.6% by placing the molecule above a dielectric surface, opening up new avenues for novel nanoscale materials design. Under current experimental conditions, the predicted molecular MC effect can be probed without substantial difficulties.

*cheng@qtp.ufl.edu

Quantum mechanical effects reduce the capacitance of a mesoscopic capacitor when the density of states is too small to completely screen the electric field, a phenomenon first reported in thin films by Luryi in 1988 [1]. Since then, quantum capacitance has been measured in a variety of experiments including recent work in graphene [2, 3]. In addition, magnetocapacitance (MC) that arises from the asymmetry in the capacitance tensor elements under field reversal [4] has been observed in magnetic field dependent measurements. Of the physical origins of MC identified so far (Landau level filling [5], band splitting due to spin-orbital coupling [6, 7], magnetoelectric interaction [8], and field-induced phase transitions [9]), only the latter two mechanisms may persist when the size of the system is reduced to a few nanometers in all three dimensions. For ultra-small systems, such as molecules or nanocrystals (collectively they can be viewed as small quantum dots), capacitance is meaningful only through the quantum definition because of the discrete energy levels, and because the geometric shape is no longer the determining factor. Instead, the energy levels near the highest occupied molecular orbital (HOMO) and the lowest unoccupied molecular orbital (LUMO) become critical. These quantities are closely related to the self-capacitance of an isolated molecule from which MC can be defined and calculated. Self-capacitance is an essential quantity in molecular junctions that exhibit Coulomb blockade effect [10, 11]. In quantum transport, self-capacitance can also be important due to charging and discharging of an isolated scattering region, processes that are beyond the scope of the steady state treatment [12, 13]. It has been worked out previously that the self-capacitance of an *N*-electron

system $C(N)$ is determined by the single-electron charging energy E_c (sometimes also called capacitive energy), which is the difference between the ionization potential (IP) and the electron affinity (EA), [14, 15]

$$E_c = \frac{e^2}{C(N)} = IP(N) - EA(N). \quad (1)$$

Equation (1) lays the foundation for our work.

In this letter, we introduce the concept of, and a detailed procedure for calculating molecular magnetocapacitance from first-principles calculations. For magnetic nano-dots whose HOMO and LUMO are determined by their magnetic states, Eq. (1) should in general depends on the magnetic state and the spin of the electron to be added and/or subtracted. The self-capacitance of the prototype particles is expected to depend on their magnetic states and can be probed experimentally. By merely switching the magnetic state of a molecular nano-magnet, one can change its capacitance. Controlling magnetic states will thus provide a simple new path to achieving MC in nano-scale materials.

Our model systems are two single molecular nano-magnets (SMM) $Mn_3O(sao)_3(O_2CMe)(H_2O)(py)_3$ and $Mn_{12}O_{12}(O_2CMe)_{16}(H_2O)_4$ (abbreviated as [Mn_3] and [Mn_{12}] respectively), and two Fe_n-C_{60}-Fe_n (n=1, 15) heterogeneous clusters. The latter are fullerene molecules with two magnetic Fe_n clusters attached on each side, which can present FM and AFM configurations. The size of the Fe_n clusters can be varied, providing excellent candidates for size-dependent studies. [Mn_3] contains three Mn^{III} ions, three pyridine ligands, one carboxylate group and a water molecule. [Mn_{12}] consists a [$Mn^{IV}_4O_4$] cube at the center, a ring of eight Mn^{III} and eight O^{2-} ions, and 16 carboxylate groups, plus 4

water molecules. Both are stable at room temperature and can be used in single-molecule tunneling junctions [16-20]. A rich array of magnetic states or spin states has been observed. Theoretically, [Mn_3] can be in an *S*=6 high-spin (HS) state or in an *S*=2 low-spin (LS) state depending on the relative spin orientations of the three Mn^{III} ions. The LS state is observed as the ground state in experiment [21]. In [Mn_{12}], ferromagnetic ordered Mn^{III} ions are aligned anti-parallel to Mn^{IV} ions, making an *S*=10 ground state. In this paper, we always refer the ground state, if it is not the one with the maximum spin polarization, as the LS state, and the fully ferromagnetic state (S=22 for [Mn_{12}]) as the HS state. Tunneling transport through an [Mn_{12}] single-electron transistor has been studied using density functional theory [22, 23]. These systems can be viewed as zero-dimensional quantum dots. Following Eq. (1), we relate potential energy change upon charging and discharging to the capacitance of the system, and the calculation of the potential energy change is based on a full quantum description of electrons coupled with molecular configurations.

We define IP and EA for each magnetic particle as: $IP = \min\left\{IP_{\uparrow}, IP_{\downarrow}\right\}$, and $EA = \max\left\{EA_{\uparrow}, EA_{\downarrow}\right\}$, that is, IP is the *least* energy cost and EA is the *most* energy gain when we add and subtract an electron with a spin parallel or anti-parallel to the net moment of the nano-magnet. With this important *least-most energy principle*, we examine the physical properties of nano-magnet systems. The basic procedure consists of 1) optimizing the molecular configuration and obtaining the electronic structure and magnetic configuration, 2) adding and/or subtracting an electron of spin-up and/or spin-down followed by optimization, 3)

extracting E_c according to *the least-most energy* principle, and 4) calculating the magnetic quantum capacitance using Eq. (1). The magnetocapacitance is defined as,

$$MC = 2(C_{HS} - C_{LS}) / \left(C_{LS} + C_{HS}\right), \quad (2)$$

in analogy to the definition of magnetoresistance. Here C_{HS} and C_{LS} are the capacitances of HS and LS states. Note that the capacitance and MC defined in Eqs. (1)-(2) apply to isolated systems. Polarizability of the molecule, discussed in supporting materials, is often confused with the capacitance but does not play a role in these equations.

The ionization potential and electron affinity of the [Mn_3] and [Mn_{12}] SMMs, and the Fe_n-C_{60}-Fe_n systems are calculated from the Kohn-Sham density functional theory [24] using the spin-polarized Perdew-Burke-Ernzerhof (PBE) exchange-correlation functional in the PAW[25, 26] pseudopotential formalism implemented in the plane-wave based VASP[27, 28] package. The [Mn_3] and [Mn_{12}] molecules are placed in a 35 Å by 35 Å by 35 Å unit cell for isolation from neighboring molecules for both neutral and charged systems, while the size of the unit cell for Fe_n-C_{60}-Fe_n is 40 Å by 40 Å by 40 Å. One k point, the Γ-point, is used for the Brillouin zone integration[29]. The plane-wave energy cutoff is 500 eV. Thresholds for self-consistency and structure optimization are set as 10^{-5} eV and 0.02 eV/Å, respectively. On-site U is included for the Mn d-electrons for the DFT+U calculation [30]. The spin-orbit coupling (SOC) calculation is performed with the direction of the magnetic moment fixed.

Table 1 summarizes the magnetocapacitance and switching field estimated via $B = \Delta E / g\mu_B \Delta M$ of all systems considered, including [Mn_{12}] and [Mn_3] in neutral and ionic states, and Fe_n-C_{60}-Fe_n (n=1 and 15). The neutral [Mn_{12}] molecule gives the highest MC, 11.3%. The MC of $[Mn_{12}]^+$ and $[Mn_{12}]^-$ ions are determined to be negative. The MC of [Mn_3] and Fe_n-C_{60}-Fe_n systems range from 3% to 6%. The switching field is as high as around 200 T for all [Mn_{12}] systems, due to the large energy difference between the HS and LS states. The fields for [Mn_3] and $[Mn_3]^+$ are 40 T and 57 T, respectively. For Fe_n-C_{60}-Fe_n systems, the switching field is 124 T for n=1, but decreases with increasing ΔM, down to 1.2 T for n=15.

In the following discussion we focus on [Mn_3], possibly the best candidate for first proof-of-principle experimental measurement. Figure 1 shows the optimized structure of a [Mn_3] molecule. The whole molecule has the C_{2v} symmetry. Three pyridine ligands are attached to Mn^{III} ions above the $[Mn^{III}]_3$-plane. Below the $[Mn^{III}]_3$ plane, one carboxylate group is shared by Mn2 and Mn3, which are equivalent, while a water molecule is attached to Mn1, distinguishing it from the other two Mn atoms. The other atoms lie almost completely within the $[Mn^{III}]_3$-plane. The largest deviation from the plane is the position of the middle oxygen (O1) atom [21, 31] (0.39 Å above the plane, in good agreement with the experimental value of 0.33 Å). Both the HS and LS states show very similar structures after optimization.

There are three low-spin configurations, LS1=(down, up, up), LS2=(up, down, up) and LS3=(up, up, down), the latter two being degenerate due to

symmetry. LS2 is 21 meV lower in energy than LS1 by and 37 meV lower than the HS state, in good agreement with previous calculations [31]. There is a multiconfigurational correction to the energy due to the mixing of the degenerate spin states [32]. This correction can be evaluated using a Heisenberg Hamiltonian extracted from the exchange interactions, and is found to slightly increase the energy difference between the S=6 and S=2 states to 44 meV. Details of the calculation are given in the supplementary materials.

Next we proceed to step 2 to calculate the energy changes in various initial and final states of [Mn_3] upon adding or removing an electron. We consider only the most stable LS state. Anions (cations) were prepared by adding (removing) a spin-up or a spin-down electron such that ions of all possible different spin states were created. Table 2 shows the energies of the neutral molecule, cation and anion of both HS and LS states. We denote anion_up and anion_down as gaining a spin-up and a spin-down electron, respectively. Similarly, cation_up and cation_down refer to losing a spin-up and spin-down electron, respectively. Structural optimizations were performed for all states. The relaxation energies, defined as the energy difference before and after structural relaxation for a charged system from the neutral structure, are 33, 57, 78 and 54 meV for anion_up, anion_down, cation_up and cation_down in the HS state, while those of LS states are 88, 86, 79 and 73 meV. As shown, the HS state prefers to absorb a spin-up electron over a spin-down electron by 75 meV, and favors losing a spin-up electron rather than a spin-down one by 592 meV. In contrast to the HS state, the LS state, which is the ground state, prefers to gain a

spin-down electron over a spin-up electron by 45 meV. However, it prefers to lose a spin-up electron than a spin-down one by 80 meV.

Step 3 is to follow *the least-most energy* principle and select the most stable anion and cation states for calculations of ionization potential and electron affinity. Table 3 lists the ionization potential (*IP*), electron affinity (*EA*), capacitance (*C*) and charging energy (E_c) of both HS and LS states (Step 4 followed immediately once *IP* and *EA* were identified). Charging energy and capacitance were calculated according to Eq. (1). It can been seen that the HS state is 175 meV lower in *IP* and 75 meV higher in *EA* than the LS state, resulting in a capacitance of the HS state that is 6% (or 0.247×10^{-20} F) higher than in the LS state (or 6% magnetocapcitance), and a charging energy that is 260 meV lower than those of the LS state.

The difference in E_c between the HS and LS states constitutes the physical foundation for the concept of quantum magnetocapacitance. Without a magnetic field, the molecule stays in the LS ground state, which has a high charging energy. The system can be switched into the HS state, which has a lower charging energy, by applying a sufficiently high magnetic field, resulting in a change in the quantum capacitance of the molecule, or a quantum magnetocapacitance. We estimate the magnitude of the switching magnetic field via $B = \Delta E / g\mu_B \Delta M$, where ΔE is the energy difference between HS and LS states (37 meV), ΔM is the magnetic moment difference, μ_B=0.058 meV/T, and the *g*-factor is equal to 2. With these values, the switching magnetic field is approximately 40 T at 0 K for [Mn_3].

It is important to understand the microscopic origin of the charging energy difference between HS and LS states. We thus calculate the spatial distribution of total charge difference between the neutral and the charged [Mn_3] for both anions and cations in the HS and LS states. In Fig. 2, panels (a) and (b) depict the charge difference between neutral molecule and cation, and that between the anion and the neutral molecule in the HS state, and panel (c) and (d) show those in the LS state. By comparing Fig. 2 with electron orbitals (supplementary materials Fig. A), we find that the charge density difference is mainly from the highest occupied electron orbitals (HOMOs). Note that the electron in the HOMO of the neutral molecule is the electron lost in the ionization process, and the electron in the HOMO of the anion is the electron gained when attaching an electron. Panels (a) and (c) (corresponding to HOMOs of the HS and LS neutral atoms, respectively) show significant difference between the HS and the LS cations, especially at the Mn2 site. Drastically different distributions of the lost electron between the HS and the LS states lead to a relatively large difference in *IP* (175 meV). Meanwhile, panels (b) and (d) (correspond to the HOMOs of the HS and the LS anions, respectively) display some similarities, especially on all three Mn atoms, which explains the relatively small difference in *EA* (75 meV). The main difference is around the center oxygen atom.

The mechanism of quantum magnetocapacitance is therefore clear: the charging process in a magnetic system depends on the magnetic state of the system and also on the spin of the incoming and outgoing electrons. The capacitance can be controlled by external magnetic field, which changes the spin

configuration of a quantum dot. The proposed controllable magnetic quantum capacitance is fundamentally different from tuning the quantum capacitance by utilizing Landau levels [33] where the system itself is non-magnetic and thus the capacitance is not spin dependent. As the size of a system is reduced, it becomes harder and harder to utilize Landau levels. To generate one magnetic flux quantum through a quantum dot of 2×2 nm^2 in cross-sectional area, such as [Mn_3] molecule (in the *x*-*y* plane), the required magnetic field is 500 Tesla. The switching field for our model molecule of about 40 T does not allow even one electron in each Landau level, and the capacitance cannot be modulated through Landau levels under such a field.

Next we consider some of the factors that can affect the switching field. First, the effect of the spin-orbit coupling (SOC) is estimated by calculating magnetic anisotropy barriers (MAB) of [Mn_3], which are 2.7 meV and 2.5 meV for LS and HS states, respectively, and 5.0 meV and 4.7 meV for [Mn_{12}], respectively. The MAB of [Mn_{12}] LS state, 5.0 meV (or 58.0 K), is close to the experiment and previous DFT studies [34-38]. These values are much lower than the difference of charging energies between HS and LS states (270 meV for [Mn_{12}] and 205 meV for [Mn_3]). The SOC slightly changes the energy difference between HS and LS states thus the switching field, but has negligible effect on MC. With the SOC included, the switching field decreases by 3 T for both of [Mn_3] and [Mn_{12}].

We also investigate the effect of on-site U using DFT+U method. A value of $U=2$ eV combined with PBE (equivalent to $U=4$eV in LDA+U), is used to

reproduce the experimental HOMO-LUMO gap and magnetic exchange [39]. For [Mn_3] molecule, MC remains 6.0% and the switching field is reduced to 17 T from 40 T. For [Mn_{12}], DFT+U also lowers the energy difference and hence reducing the switching field by 70%, with a small effect on MC (9.0%). Overall, the on-site *U* gives a smaller switching field, and maintains the MC effect. More details are presented in supplementary materials.

Finally, the switching field can also be tuned by varying the organic ligands. Such a calculation is beyond the scope of this work. Experimentally, it was found that the $[NEt_4]_3Mn_3Zn_2(salox)_3O(N_3)_8]\cdot MeOH$ molecule needs 28 T to switch from LS to HS [40].

Substrate can have a large impact on MC. To study this effect, we place the [Mn_3] molecule 3 Å above an *h*-BN surface measured from the bottom of the molecule an energy minimum search. The BN surface enhances the MC to 9.6% from 6% for the isolated molecule, without affecting the switching field. Other substrates are also studied, showing a strong dependence of the MC on the substrate (see supplementary materials). For example, the MC of the [Mn_3] molecule on a metal surface based on image charge analysis is 12%. These results indicate that a thorough search for optimal substrates as well as organic ligands will likely lead to a rich array of discoveries.

The molecular magnetocapacitance is best exploited through the Coulomb blockade effect. It has been proposed [41, 42] that a small spin-dependence of the charging energy of a quantum dot can lead to a giant Coulomb blockade

magnetoresistance effect. SMMs and magnetic nanostructures that demonstrate magnetocapacitance are the perfect candidates for realizing this effect.

In summary, we have demonstrated the concept of molecular magnetocapacitance, that the capacitance of nano-magnet can be spin-dependent. As an example, the [Mn_3] SMM has been investigated by first-principles calculations. The magnetocapacitance of a stand-alone [Mn_3] molecule is determined as 6%, which is enhanced to 9.6% in the presence of a dielectric BN substrate, and a 40 T magnetic field is needed to switch the molecule from low-spin state to high-spin state. The proposed Fe_n-C_{60}-Fe_n systems are also good candidates for molecular magnetocapacitance, in which the switching field can be lowered by increasing the magnetic moment. Our findings on SMMs and Fe_n-C_{60}-Fe_n suggest that an exhaustive search for candidate systems can be very fruitful. Future synthesis of SMM guided by the energy principle may hold the key for realizing quantum dots with capacitance that is tunable using magnetic field under 1 T.

Acknowledgement: This work is supported by U. S. DOE/BES-FG02-02ER45995. A portion of this research was conducted at CNMS sponsored at ORNL by the Scientific User Facilities Division, Office of Basic Energy Sciences, U.S. DOE. The authors also acknowledge NERSC and UF-HPC for computing resources. We thank Dr. Junjie Liu for fruitful discussions.

* Corresponding author: cheng@qtp.ufl.edu

1. S. Luryi, Applied Physics Letters **52** (6), 501-503 (1988).

2. S. Droscher, P. Roulleau, F. Molitor, P. Studerus, C. Stampfer, K. Ensslin and T. Ihn, Appl Phys Lett **96** (15) (2010).
3. P. Nguyen and V. Berry, J Phys Chem Lett **3** (8), 1024-1029 (2012).
4. W. Chen, T. P. Smith, M. Buttiker and M. Shayegan, Phys Rev Lett **73** (1), 146-149 (1994).
5. T. P. Smith, W. I. Wang and P. J. Stiles, Phys Rev B **34** (4), 2995-2998 (1986).
6. K. T. McCarthy, A. F. Hebard and S. B. Arnason, Phys Rev Lett **90** (11) (2003).
7. Y. Yamasaki, Y. Kohara and Y. Tokura, Phys Rev B **80** (14) (2009).
8. T. Kimura, T. Goto, H. Shintani, K. Ishizaka, T. Arima and Y. Tokura, Nature **426** (6962), 55-58 (2003).
9. R. P. Rairigh, G. Singh-Bhalla, S. Tongay, T. Dhakal, A. Biswas and A. F. Hebard, Nat Phys **3** (8), 551-555 (2007).
10. J. Park, A. N. Pasupathy, J. I. Goldsmith, C. Chang, Y. Yaish, J. R. Petta, M. Rinkoski, J. P. Sethna, H. D. Abruna, P. L. McEuen and D. C. Ralph, Nature **417** (6890), 722-725 (2002).
11. W. A. Schoonveld, J. Wildeman, D. Fichou, P. A. Bobbert, B. J. van Wees and T. M. Klapwijk, Nature **404** (6781), 977-980 (2000).
12. A. Donarini, M. Grifoni and K. Richter, Phys Rev Lett **97** (16) (2006).
13. A. Nitzan and M. A. Ratner, Science **300** (5624), 1384-1389 (2003).
14. G. J. Iafrate, K. Hess, J. B. Krieger and M. Macucci, Phys Rev B **52** (15), 10737-10739 (1995).
15. V. V. Shorokhov, E. S. Soldatov and S. P. Gubin, Journal of Communications Technology and Electronics **56** (3), 326-341 (2011).
16. H. B. Heersche, Z. de Groot, J. A. Folk, H. S. J. van der Zant, C. Romeike, M. R. Wegewijs, L. Zobbi, D. Barreca, E. Tondello and A. Cornia, Physical Review Letters **96** (20) (2006).
17. M. H. Jo, J. E. Grose, K. Baheti, M. M. Deshmukh, J. J. Sokol, E. M. Rumberger, D. N. Hendrickson, J. R. Long, H. Park and D. C. Ralph, Nano Letters **6** (9), 2014-2020 (2006).
18. S. Voss, O. Zander, M. Fonin, U. Rudiger, M. Burgert and U. Groth, Physical Review B **78** (15) (2008).
19. F. Haque, M. Langhirt, E. del Barco, T. Taguchi and G. Christou, Journal of Applied Physics **109** (7) (2011).
20. T. Komeda, H. Isshiki, J. Liu, Y. F. Zhang, N. Lorente, K. Katoh, B. K. Breedlove and M. Yamashita, Nat Commun **2** (2011).
21. C. J. Millos, A. G. Whittaker and E. K. Brechin, Polyhedron **26** (9-11), 1927-1933 (2007).
22. L. Michalak, C. M. Canali, M. R. Pederson, M. Paulsson and V. G. Benza, Phys Rev Lett **104** (1) (2010).
23. S. Barraza-Lopez, K. Park, V. Garcia-Suarez and J. Ferrer, Phys Rev Lett **102** (24) (2009).
24. W. Kohn and L. J. Sham, Physical Review **140** (4A), 1133-& (1965).
25. P. E. Blochl, O. Jepsen and O. K. Andersen, Phys Rev B **49** (23), 16223-16233 (1994).
26. G. Kresse and D. Joubert, Phys Rev B **59** (3), 1758-1775 (1999).
27. G. Kresse and J. Furthmuller, Phys Rev B **54** (16), 11169-11186 (1996).

28. G. Kresse and J. Furthmuller, Computational Materials Science **6** (1), 15-50 (1996).
29. H. J. Monkhorst and J. D. Pack, Phys Rev B **13** (12), 5188-5192 (1976).
30. V. I. Anisimov, F. Aryasetiawan and A. I. Lichtenstein, J Phys-Condens Mat **9** (4), 767-808 (1997).
31. J. Cano, T. Cauchy, E. Ruiz, C. J. Milios, C. C. Stoumpos, T. C. Stamatatos, S. P. Perlepes, G. Christou and E. K. Brechin, Dalton Transactions (2), 234-240 (2008).
32. A. V. Postnikov, J. Kortus and M. R. Pederson, Phys Status Solidi B **243** (11), 2533-2572 (2006).
33. L. A. Ponomarenko, R. Yang, R. V. Gorbachev, P. Blake, A. S. Mayorov, K. S. Novoselov, M. I. Katsnelson and A. K. Geim, Physical Review Letters **105** (13) (2010).
34. S. Barraza-Lopez, M. C. Avery and K. Park, Phys Rev B **76** (22) (2007).
35. A. L. Barra, D. Gatteschi and R. Sessoli, Phys Rev B **56** (13), 8192-8198 (1997).
36. S. Hill, J. A. A. J. Perenboom, N. S. Dalal, T. Hathaway, T. Stalcup and J. S. Brooks, Phys Rev Lett **80** (11), 2453-2456 (1998).
37. J. R. Friedman, M. P. Sarachik, J. Tejada and R. Ziolo, Phys Rev Lett **76** (20), 3830-3833 (1996).
38. M. R. Pederson and S. N. Khanna, Phys Rev B **60** (13), 9566-9572 (1999).
39. D. W. Boukhvalov, M. Al-Saqer, E. Z. Kurmaev, A. Moewes, V. R. Galakhov, L. D. Finkelstein, S. Chiuzbaian, M. Neumann, V. V. Dobrovitski, M. I. Katsnelson, A. I. Lichtenstein, B. N. Harmon, K. Endo, J. M. North and N. S. Dalal, Phys Rev B **75** (1) (2007).
40. J. Liu, C. Koo, A. Amjad, P. L. Feng, E. S. Choi, E. del Barco, D. N. Hendrickson and S. Hill, Phys Rev B **84** (9) (2011).
41. X. G. Zhang, Z. C. Wen, H. X. Wei and X. F. Han, Phys Rev B **81** (15) (2010).
42. X. G. Zhang and T. Xiang, International Journal of Quantum Chemistry **112** (1), 28-32 (2012).

Fig.1: Optimized structure of [Mn_3] molecules. Panel (a) is top view and (b) is side view. Mn atoms are in purple. O atoms are in red. Blue spheres are N atoms. Grey and blue-green sticks stand for C and H atoms.

(a) (b)

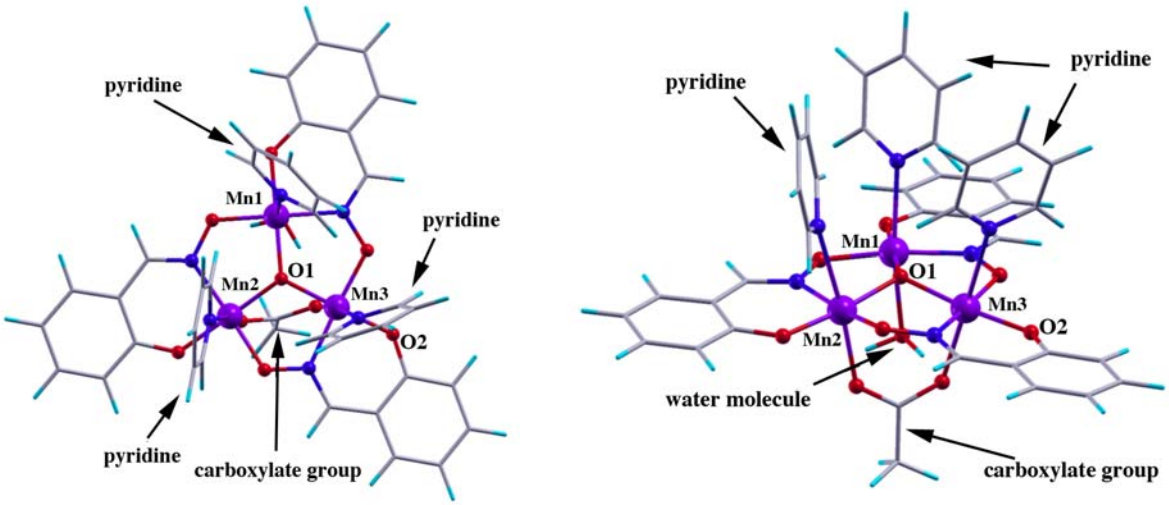

Fig. 2: Isosurfaces of charge difference (a) between neutral molecule and cation of high-spin state, (b) between anion and neutral molecule of high-spin state, (c) between neutral molecule and cation of low-spin state and (d) between anion and neutral molecule of low-spin state. Isovalue is 0.015 e/Å^3.

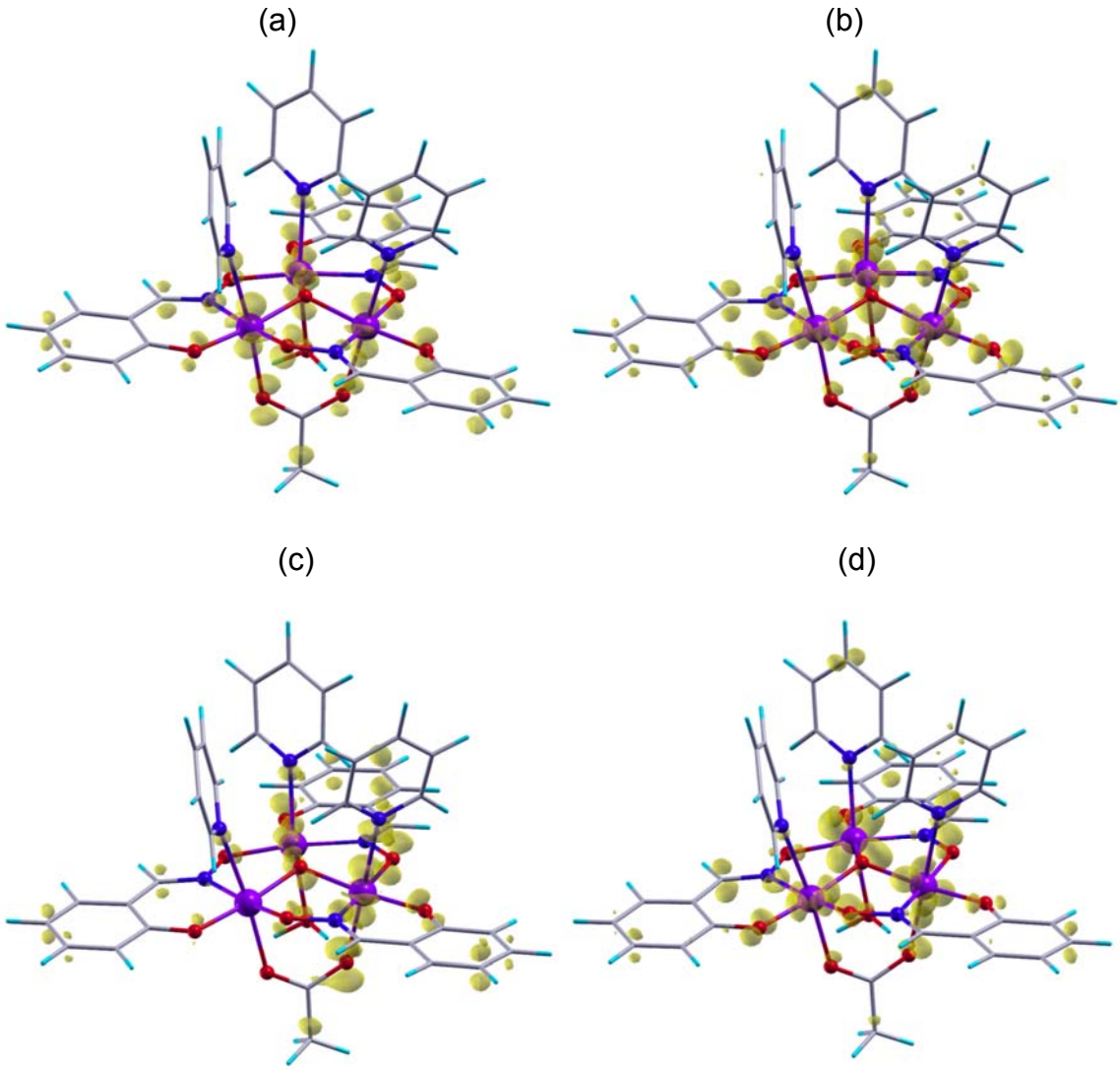

Table 1: The molecular magenetocapacitance and the estimated switching field of all considered systems.

Molecule/Ion	MC%	Switching **B** (T)
Mn_{12}	11.3	241
Mn_{12}^{+}	-3.2	196
Mn_{12}^{-}	-9.4	190
Mn_3	6.1	40
Mn_3^{+}	4.1	57
Fe_1-C_{60}-Fe_1	6.0	124
Fe_{15}-C_{60}-Fe_{15}	3.6	1.2

Table 2: Energies of neutral case, cation and anion of both HS and LS states. Adding/removing one spin up/down electron are all considered. The energy of neutral LS state (ground state) is set to be 0.

	High-spin state		Low-spin state	
	Energy (eV)	Magnetization (μ_B)	Energy (eV)	Magnetization (μ_B)
neutral	0.037	12	0	4
anion_up	**-1.627**	13	-1.544	5
anion_down	-1.552	11	**-1.589**	3
cation_up	**5.677**	11	**5.825**	3
cation_down	6.269	13	5.905	5

Table 3: Ionization potential (IP), electron affinity (EA), capacitance (C) and charging energy (E_c) of both HS and LS states.

	High-spin state	Low-spin state	$2(HS-LS)/(HS+LS)$
I P(eV)	5.640	5.825	-3%
EA (eV)	1.664	1.589	4%
C (10^{-20} F)	4.029	3.782	6%
E_c (eV)	3.976	4.236	-6%